Signal Processing 158 (2019) 4–14

Contents lists available at ScienceDirect

Signal Processing

journal homepage: www.elsevier.com/locate/sigpro

A cost-effective nonlinear self-Interference canceller in full-duplex direct-conversion transceivers

Zhe Li[a], Yili Xia[a,*], Wenjiang Pei[a,*], Danilo P. Mandic[b]

[a] School of Information Science and Engineering, Southeast University, Nanjing, 210096, P. R. China
[b] Department of Electrical and Electronic Engineering, Imperial College London, London, SW7 2AZ, UK

ARTICLE INFO

Article history:
Received 10 July 2018
Revised 5 November 2018
Accepted 17 December 2018
Available online 18 December 2018

Keywords:
Full-duplex transceiver
Self-interference
I/q imbalance
PA Nonlinearity
Complex dual channel estimation
Dual channel nonlinear complex least-mean-square (DC-NCLMS)
Widely linear complex LMS (WL-CLMS)

ABSTRACT

Cancellation of self-interference (SI) arising due to hardware nonidealities is a key issue in the design of mobile-scale full-duplex devices in future full-duplex (FD) communications. To efficiently address this issue in the baseband, we propose a cost-effective adaptive digital SI cancellation scheme for FD direct-conversion transceivers (DCTs) in the presence of major circuit imperfections, such as frequency-dependent I/Q imbalance, power amplifier (PA) distortion, thermal noise and quantization noise. This is achieved by employing a recent complex dual channel estimation (CDC) framework which offers low computational complexity in the widely nonlinear model fitting task which underpins this problem, to yield a dual channel nonlinear complex least-mean-square (DC-NCLMS) based SI canceller. For rigor, a unified theoretical evaluation is further performed to illustrate the second order performance optimality and low computation requirements of DC-NCLMS in both the transient and steady state stages. Further, for enhanced convergence, the proposed SI cancellation structure is equipped with an affine projection based scheme and a prewhitening procedure. Simulations in practical FD DCT settings, compliant with orthogonal frequency division multiplexing (OFDM)-based IEEE 802.11ac standard, support the findings.

Notation

Lowercase letters denote scalars, a, boldface letters column vectors, $\mathbf{a}$, and boldface uppercase letters matrices, $\mathbf{A}$. An $N \times N$ identity matrix is denoted by $\mathbf{I}_N$. The superscripts $(\cdot)^*$, $(\cdot)^T$, $(\cdot)^H$ and $(\cdot)^{-1}$ denote respectively the complex conjugation, transpose, Hermitian transpose and matrix inversion operators. The operator $\mathrm{Tr}\{\cdot\}$ returns the trace of a matrix, while the symbols $\star$, $\otimes$, $\|\cdot\|$ respectively denote the convolution, Kronecker product and Euclidean norm operators. The statistical expectation operator is denoted by $E[\cdot]$, matrix determinant by $\det[\cdot]$, while the operators $\Re\{\cdot\}$ and $\Im\{\cdot\}$ extract respectively the real and imaginary parts of a complex variable and $j = \sqrt{-1}$. Matrix vectorization is designated by $\mathrm{vec}\{\cdot\}$, which returns a column vector formed by stacking the successive columns of matrix, while its inverse operation, which restores the matrix from the its vectorized form, is denoted by $\mathrm{vec}^{-1}\{\cdot\}$. The extraction of matrix diagonal elements into a vector is denoted by $\mathrm{diag}\{\cdot\}$. The operator $\lambda_{\max}[\cdot]$ returns the largest positive eigenvalue of a matrix.

1. Introduction

The exponential growth in the number of wireless devices and mobile data usage poses critical challenges to the next generation communication relates to both large capacity enhancement and improvements in the spectral and energy efficiency [1]. To this end, the full-duplex (FD) technology, which aims to achieve a doubled radio-link data rate by transmitting and receiving simultaneously and bidirectionally at the same center frequency, has recently received plenty of attention [2,3]. A major challenge in the design of a full-duplex transceiver is the attenuation of the self-interference (SI), a strong transmit signal coupled into the receiver (Rx) path. Since the transmitter (Tx) and Rx chains are closely intertwined at an FD transceiver node, the SI power leakage from the Tx chain can be even 50 dB to 110 dB higher than the Rx sensitivity level in either the WiFi or cellular scenarios [4].

Recent successful experimental demonstrations [5–12], based on the wireless open access research platform (WARP), have opened the possibility for a practical realisation of FD technology, however, these contributions, such as full-duplex relaying techniques [8,9], primarily focus on the backhaul nodes in FD networks. Given that both base stations and far-end devices running in FD mode are essential for the exploitation of the full available degrees of freedom in FD technology [13], more attention has been paid to

* Corresponding authors.
E-mail addresses: lizhe_nanjing@seu.edu.cn (Z. Li), yili_xia@seu.edu.cn (Y. Xia), wjpei@seu.edu.cn (W. Pei), d.mandic@imperial.ac.uk (D.P. Mandic).

https://doi.org/10.1016/j.sigpro.2018.12.012
0165-1684/

the design of mobile-scale FD devices [14]. A popular hardware solution in wireless devices in the half-duplex era is the well-known direct-conversion-transceiver (DCT) architecture [15,16]. However, due to the stringent constraints imposed by mobile devices, e.g., small size, low cost and low power consumption, employing DCTs in FD mobile devices would fail to meet the requirements of SI cancellation challenge.

Existing solutions [5–7,10–12,17] typically achieve the mitigation of SI in both the analog and digital stages, so as to attain a sufficient signal-to-interference-plus-noise-ratio (SINR). The purpose of analog cancellation is to prevent the SI power from the saturation area of the Rx low-noise amplifier (LNA), and at the same time, to ensure the power difference between the SI residual and the received signal of interest does not exceed the dynamic range of the analog-to-digital converter (ADC) [18]. Further digital baseband cancellation is the next imperative, as the residual SI components and radio-frequency (RF) circuit nonidealities, including power amplifier (PA) distortion, I/Q imbalance and phase noise, reduce the degree of the desirable SI attenuation. To this end, our focus in this work in on improving digital SI cancellation for FD DCTs

The digital SI cancellation problem in FD DCTs, in the context of main RF front-end nonidealities, such as PA nonlinearity and I/Q imbalance, has just emerged in the literature [19–22]. Impact of these imperfections on digital SI cancellation are studied in [19], where a widely linear (WL) digital SI canceller [23,24] was developed for this purpose and its parameters were estimated using block-based methods which take into account of the original SI component, and its image byproduct resulting from Tx and Rx frequency-dependent I/Q imbalance. Upon realizing that in practice adaptive estimation algorithms have key advantages over block-based ones, in [20] the augmented complex least mean square (ACLMS) adaptive filtering algorithm [25–27] was employed within a DSP-assisted analog SI cancellation process, and its theoretical SI cancellation capability in the presence of Tx and Rx IQ imbalance was evaluated. However, neither the result in [19] nor that in [20] was able to achieve the optimal solution in the presence of nonlinear higher-order intermodulation (IMD) interference, for example when the transmit power of the FD DCT is high. To address this issue, our previous work [28] introduces an augmented nonlinear CLMS (ANCLMS) based SI canceller for a joint cancellation of both the linear and nonlinear SI components, achieved by virtue of widely nonlinear model fitting. This proof of concept strictly produced a rigorous theoretical framework but without consideration of computational complexity.

Independently, in adaptive filtering literature, a cost-effective complex dual channel (CDC) estimation framework was recently proposed in [29,30] which reduces computational complexity of ACLMS by exploiting the duality between complex-valued signal representations and their bivariate-real counterparts [31]. Here we embark upon this possibility of computationally efficient WL modelling and proceed to introduce a novel framework of understanding the FD DCT SI cancellation task from a bivariate-real perspective. This is achieved by proposing a dual channel nonlinear complex least-mean-square (DC-NCLMS) canceller and a convenient factorisation of the mean square error (MSE) function used in the ANCLMS based SI canceller [28], followed by two low-computational cost independent optimisation processes. Rigourous mean and mean square convergence and steady state performance evaluations are next conducted, to ensure a second order optimality and low computational complexity of the proposed canceller in the context of widely nonlinear modeled SI cancellation for FD DCTs. To further speed up convergence of the proposed DC-NCLMS SI canceller, both an affine projection based adaptive scheme and a data prewhitening one are provided. Simulations in practical FD DCT settings validate the theoretical results.

2. Baseband modelling of FD DCTs

Fig. 1 shows a typical FD DCTs architecture. In the FD mode of operation, one common antenna is shared by both Tx and Rx, and a circulator is employed to isolate the transmitting signal path from that received from the far end. This structure is designed to provide a certain amount of passive isolation between the Tx and the Rx paths, and hence, it is regarded as a cost-effective and energy-saving way to design mobile FD transceivers. However, the effects of leakage of the circulator, single-path reflection from the antenna, and multi-path interference from surrounding environment introduce a large amount of residual self-interference, which requires further mitigation. This mitigation is usually achieved by two consecutive modules - RF cancellation circuitry and digital baseband SI suppressor. The RF canceller, as shown in Fig. 1, reconstructs and cancels the received SI by taking the output of the power amplifier (PA) as a reference, prevents over-saturation of the Rx low-noise amplifier (LNA), and relaxes the dynamic range requirements for the receiver ADC [18]. In order to further mitigate SI residuals in the output of the RF canceller, a digital SI canceller is also compulsory. Given that low-cost components are preferable for mobile DCTs, the key to the digital SI cancellation control lies in a precise baseband-equivalent system model that incorporates these prominent nonidealities within the RF circuit. Furthermore, oversampling is usually applied to the original waveform before digital-to-analog conversion (DAC) to attenuate these nonidealities [19,21,32]. Correspondingly, a timing recovery process is also required after ADC in order to convert the digitised data to its original sampling rate. In Fig. 1, the baseband equivalent discrete-time SI signal, $x(n)$, which is also the input of the digital SI canceller, is assumed to be critically sampled, for the simplicity of the analysis. In this sense, $x(n)$ can be modeled as an i.i.d. proper (second-order circular) Gaussian random variable with variance σ_x^2 [33], and is inherently known to the receiver. Due to the above-mentioned imperfections, the SI signal $x(n)$ couples into to the receiver path, and after the analog SI cancellation at the RF end, at time instant n, the observed signal $d(n)$ in the baseband can be expressed in a widely nonlinear relation with $x(n)$ as [19]

$$\begin{aligned} d(n) &= \mathbf{h}^{oH}\mathbf{x}(n)+\mathbf{g}^{oH}\mathbf{x}^*(n)+\mathbf{h}_{\mathrm{IMD}}^{oH}\mathbf{x}_{\mathrm{IMD}}(n) \\ &\quad +\mathbf{g}_{\mathrm{IMD}}^{oH}\mathbf{x}_{\mathrm{IMD}}^*(n)+x_{\mathrm{SOI}}(n)+v(n)+q(n) \end{aligned} \tag{1}$$

where $\mathbf{x}(n)=[x(n),x(n-1),\ldots,x(n-M+1)]^T$ is the SI vector, $\mathbf{x}_{\mathrm{IMD}}(n)=[x_{\mathrm{IMD}}(n),x_{\mathrm{IMD}}(n-1),\ldots,x_{\mathrm{IMD}}(n-N+1)]^T$ represents the third-order intermodulation (IMD) SI vector introduced by PA distortion, and $M<N$. The element $x_{\mathrm{IMD}}(n)$ in the IMD SI vector $\mathbf{x}_{\mathrm{IMD}}(n)$ is defined as [19]

$$x_{\mathrm{IMD}}(n)=k_{\mathrm{TIQ}}^{3/2}|x(n)|^2x(n) \tag{2}$$

where k_{TIQ} is the transmitter mixer gain[1]. From (2), observe that $x_{\mathrm{IMD}}(n)$ is a zero-mean proper but non-Gaussian process, for which variance can be obtained through the Gaussian fourth order moment factorising theorem as

$$\sigma_{x_{\mathrm{IMD}}}^2=E[|x_{\mathrm{IMD}}(n)|^2]=6k_{\mathrm{TIQ}}^3\sigma_x^6 \tag{3}$$

The length-M channel impulse response (CIR) vectors $\mathbf{h}^o$ and $\mathbf{g}^o$ in (1) model respectively the overall impacts of the transmit and receive frequency-independent I/Q imbalance, PA memory and residual of RF cancellation on the SI component $\mathbf{x}(n)$ and its image $\mathbf{x}^*(n)$. In a similar way, the CIRs for the IMD SI component

[1] Although there exist distortion components beyond third-order [32], for simplicity, we here consider the third-order distortion, since in practice, it is always the strongest nonlinearity source at the PA output [19]. This is also confirmed in the manuals of commercial products in this area [34,35].

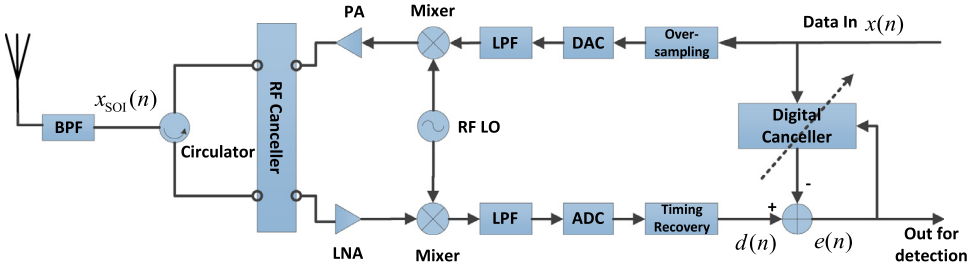

Fig. 1. The architecture of a shared-antenna FD DCT.

$x_{IMD}(n)$ and its image $x^*_{IMD}(n)$ are represented by the corresponding length-N filter coefficients $\mathbf{h}^o_{IMD}$ and $\mathbf{g}^o_{IMD}$. The symbol $v(n)$ denotes thermal noise, $q(n)$ quantization noise, which both assumed to be proper white Gaussian random process with the corresponding variances σ_v^2 and σ_q^2.

3. Adaptive nonlinear SI cancellation

From (1), the aim of an accurate digital SI cancellation process is to find an estimate of the total SI component, $x_{SI}(n)$, in the form [28]

$$x_{SI}(n) = \mathbf{h}^{oH}\mathbf{x}(n)+\mathbf{g}^{oH}\mathbf{x}^*(n)+\mathbf{h}^{oH}_{IMD}\mathbf{x}_{IMD}(n)+\mathbf{g}^{oH}_{IMD}\mathbf{x}^*_{IMD}(n) \quad (4)$$

Note that Eq. (4) contains the original SI component, $\mathbf{x}(n)$, and its image, $\mathbf{x}^*(n)$ introduced by the Tx and Rx frequency-dependent I/Q imbalance, as well as the IMD SI component, $\mathbf{x}_{IMD}(n)$ and its image interference, $\mathbf{x}^*_{IMD}(n)$, which are joint consequences of the Tx PA distortion and Rx frequency-dependent I/Q imbalance for high transmit powers. It is well understood that the powers of the IMD SI components $\mathbf{x}_{IMD}(n)$ and $\mathbf{x}^*_{IMD}(n)$ may exceed the noise floor, that is, the sum of powers of the thermal noise $v(n)$ and the quantization error $q(n)$, or may even become larger than the power of the signal of interest, $x_{SOI}(n)$ [19,28,36]. Such scenarios result in biased CIR estimates when using the conventional widely linear estimation framework, which is employed by current block-based and adaptive SI cancellation methods [19,20], this is due to insufficient degrees of freedom owing to the use of only the first two terms in (4). To address this issue, an augmented nonlinear CLMS (ANCLMS) based adaptive SI canceller has been recently proposed in [28], which employs the exact *widely nonlinear* estimation framework described in (4), to simultaneously suppress the SI and IMD SI components in a unified and rigorous way. It is important to note that this SI canceller attains the optimal theoretical solution but is computationally suboptimal as it is essentially overparameterised, and requires twice the number of coefficients compared to the complex dual channel (CDC) framework [29]. To this end, after a brief review on the original ANCLMS SI canceller, we here propose a dual-channel nonlinear CLMS (DC-NCLMS), and show that it is statistically optimal for the widely nonlinear SI cancellation paradigm, but comes with a reduced computational complexity, thus facilitating its practical applications in FD DCTs.

3.1. Original ANCLMS based SI canceller

The ANCLMS algorithm, introduced in [28], considers both the PA nonlinear distortion and frequency-dependent image interference within its estimation framework, in order to achieve a sufficient amount of SINR improvement when the nonlinear SI is not negligible. To further illustrate this idea, consider the concatenation of the SI vector $\mathbf{x}(n)$ and its higher-order interference $\mathbf{x}_{IMD}(n)$, to form a joint $(M+N)\times 1$ vector $\mathbf{x}_u(n)$, given by

$$\mathbf{x}_u(n) = [\mathbf{x}^T(n), \mathbf{x}^T_{IMD}(n)]^T \quad (5)$$

In this way, the total SI component $x_{SI}(n)$ in (4) becomes

$$x_{SI}(n) = \mathbf{h}^{oH}_u\mathbf{x}_u(n)+\mathbf{g}^{oH}_u\mathbf{x}^*_u(n) \quad (6)$$

where $\mathbf{h}^o_u = [\mathbf{h}^{oT}, \mathbf{h}^{oT}_{IMD}]^T$ and $\mathbf{g}^o_u = [\mathbf{g}^{oT}, \mathbf{g}^{oT}_{IMD}]^T$.

Eq.(6) represents a *widely nonlinear auto-regressive* (AR) model with a zero-mean non-Gaussian regressor, $\mathbf{x}_u(n)$, and an improper output $x_{SI}(n)$. Upon introducing a $(2M+2N)\times 1$ augmented column vector,

$$\mathbf{x}_b(n) = [\mathbf{x}^T_u(n), \mathbf{x}^H_u(n)]^T \quad (7)$$

Eq. (1) can be rewritten as

$$d(n) = \mathbf{w}^{oH}\mathbf{x}_b(n) + v(n) + q(n) \quad (8)$$

where $\mathbf{w}^o = [\mathbf{h}^{oT}_u, \mathbf{g}^{oT}_u]^T$. Compared with (1), the signal of interest $x_{SOI}(n)$ is not included in (8) for the simplicity of the analysis. Otherwise, this term would have been considered by the proposed SI canceller as an additional noise source which would increase its estimation variance [32].

The ANCLMS then estimates the set of system parameters, $\mathbf{w}^o$, by recursively minimising the mean square error (MSE) cost function $J(n)$, defined as

$$J(n) = E[|e(n)|^2] = E[e(n)e^*(n)] \quad (9)$$

where $e(n)$ is the instantaneous output error, given by

$$e(n) = d(n) - \mathbf{w}^H(n)\mathbf{x}_b(n) \quad (10)$$

and the augmented weight vector of ANCLMS, that is,

$$\mathbf{w}(n) = [\mathbf{h}^T_u(n), \mathbf{g}^T_u(n)]^T$$

is updated as

$$\mathbf{w}(n+1) = \mathbf{w}(n) + \mu e^*(n)\mathbf{x}_b(n) \quad (11)$$

with μ being the step-size.

3.2. Proposed DC-NCLMS based SI canceller

It was recently shown that augmented (widely linear) adaptive filtering algorithms are second order optimal for widely linear modelling scenarios [26,37,38], however, their implementations are over-parameterised. Indeed, widely linear adaptive filters can be equivalently implemented by a combination of two strictly linear complex-valued filters within a framework referred to as complex dual channel (CDC) estimation, which exhibits reduced computational complexity [29,30]. Motivated by the requirement of low complexity computation and considering that the baseband representation of the digital SI cancellation in the presence of PA distortion in (8) results in a widely nonlinear processing framework for the SI vector $\mathbf{x}(n)$, in this subsection, we next propose a novel dual-channel nonlinear adaptive digital SI canceller.

To this end, rewrite first $e(n)$ in (10) in terms of its real and imaginary components as $e(n) = \Re[e(n)] + j\Im[e(n)]$. Accordingly, the MSE $J(n)$ in (9) can be decomposed as

$$J(n) = E[|e(n)|^2] = E[e(n)e^*(n)]$$

$$= \underbrace{E\left[\left(\Re\{e(n)\}\right)^2\right]}_{J_r(n)} + \underbrace{E\left[\left(\Im\{e(n)\}\right)^2\right]}_{J_i(n)} \tag{12}$$

where $\Re\{e(n)\}$ and $\Im\{e(n)\}$ can be further expressed as

$$\begin{aligned}\Re\{e(n)\} &= \Re\{d(n) - \mathbf{w}^H(n)\mathbf{x}_b(n)\}\\ &= \Re\{d(n) - \mathbf{h}_u^T(n)\mathbf{x}_u(n) - \mathbf{g}_u^T(n)\mathbf{x}_u^*(n)\}\\ &= \Re\{d(n)\} - \left(\Re\{\mathbf{h}_u(n) + \mathbf{g}_u(n)\}\right)^T\Re\{\mathbf{x}_u(n)\}\\ &\quad + \left(\Im\{\mathbf{h}_u(n) - \mathbf{g}_u(n)\}\right)^T\Im\{\mathbf{x}_u(n)\}\end{aligned} \tag{13}$$

and

$$\begin{aligned}\Im\{e(n)\} &= \Im\{d(n) - \mathbf{w}^H(n)\mathbf{x}_b(n)\}\\ &= \Im\{d(n) - \mathbf{h}_u^T(n)\mathbf{x}_u(n) - \mathbf{g}_u^T(n)\mathbf{x}_u^*(n)\}\\ &= \Im\{d(n)\} - \left(\Im\{\mathbf{h}_u(n) + \mathbf{g}_u(n)\}\right)^T\Re\{\mathbf{x}_u(n)\}\\ &\quad - \left(\Re\{\mathbf{h}_u(n) - \mathbf{g}_u(n)\}\right)^T\Im\{\mathbf{x}_u(n)\}\end{aligned} \tag{14}$$

Remark 1. The real and imaginary parts of the instantaneous error $e(n)$ of ANCLMS in (10) can be considered as outputs of two individual adaptive filters in (13) and (14), whereby the weight vectors for the direct and image CIRs, i.e., $\mathbf{h}_u(n)$ and $\mathbf{g}_u(n)$, are half the length of $\mathbf{w}(n)$ used in ANCLMS in (10), but provide the same number of degrees of freedom.

Now, by minimising the two cost functions $J_r(n)$ and $J_i(n)$ in (12) independently, we can find the estimate of the summed SI signal $x_{\text{SI}}(n)$. For a more comprehensive understanding of each individual estimator, a new pair of optimal weights $\mathbf{w}_{\text{cr}}^{\text{o}}$ and $\mathbf{w}_{\text{ci}}^{\text{o}}$ is first introduced to equivalently represent the end-to-end CIRs $\mathbf{h}_u^{\text{o}}$ and $\mathbf{g}_u^{\text{o}}$ in (8), given by

$$\mathbf{w}_{\text{cr}}^{\text{o}} = \mathbf{h}_u^{\text{o}} + \mathbf{g}_u^{\text{o}^*} \tag{15}$$

$$\mathbf{w}_{\text{ci}}^{\text{o}} = \mathbf{h}_u^{\text{o}} - \mathbf{g}_u^{\text{o}*} \tag{16}$$

Taking (15) and (16) back into (8), the observed signal $d(n)$ can be rewritten as

$$\begin{aligned}d(n) &= \frac{\mathbf{w}_{\text{cr}}^{\text{o}H} + \mathbf{w}_{\text{ci}}^{\text{o}H}}{2}\mathbf{x}_u(n) + \frac{\mathbf{w}_{\text{cr}}^{\text{o}T} - \mathbf{w}_{\text{ci}}^{\text{o}T}}{2}\mathbf{x}_u^*(n) + v(n) + q(n)\\ &= \Re\{\mathbf{w}_{\text{cr}}^{\text{o}H}\mathbf{x}_u(n)\} + j\Im\{\mathbf{w}_{\text{ci}}^{\text{o}H}\mathbf{x}_u(n)\} + v(n) + q(n)\end{aligned} \tag{17}$$

which gives the widely nonlinear SI cancellation model within the CDC framework.

We can now use the two weight vectors, $\mathbf{w}_{\text{cr}}(n)$ and $\mathbf{w}_{\text{ci}}(n)$, to track the corresponding $\mathbf{w}_{\text{cr}}^{\text{o}}$ and $\mathbf{w}_{\text{ci}}^{\text{o}}$, so as to decouple $\Re\{e(n)\}$ and $\Im\{e(n)\}$ in (13) and (14), to give

$$\Re\{e(n)\} = \Re\{d(n)\} - \Re\{\mathbf{w}_{\text{cr}}^H(n)\mathbf{x}_u(n)\} \tag{18}$$

$$\Im\{e(n)\} = \Im\{d(n)\} - \Im\{\mathbf{w}_{\text{ci}}^H(n)\mathbf{x}_u(n)\} \tag{19}$$

The proposed DC-NCLMS SI canceller is then formed by performing two independent gradient descent weight update processes, denoted as NCLMSr and NCLMSi, simultaneously. The NCLMSr aims to minimise the MSE cost function $J_r(n)$ along the real error channel, and is defined as

$$\begin{aligned}J_r(n) &\triangleq E[(\Re\{e(n)\})^2]\\ &= E[(\Re\{d(n)\} - \Re\{\mathbf{w}_{\text{cr}}^H(n)\mathbf{x}_u(n)\})^2]\end{aligned} \tag{20}$$

The weight update is found based on the conjugate derivative $\nabla J_r(n) = \partial J_r(n)/\partial \mathbf{w}_{\text{cr}}^*(n)$, given by [39],

$$\text{NCLMSr}: \quad \mathbf{w}_{\text{cr}}(n+1) = \mathbf{w}_{\text{cr}}(n) + \mu\Re\{e_{\text{cr}}(n)\}\mathbf{x}_u(n) \tag{21}$$

where

$$e_{\text{cr}}(n) = d(n) - \mathbf{w}_{\text{cr}}^H(n)\mathbf{x}_u(n) \tag{22}$$

In a similar way, within NCLMSi, the MSE cost function $J_i(n)$ in the imaginary error channel can be derived from (12) and (14) as

$$\begin{aligned}J_i(n) &\triangleq E[(\Im\{e(n)\})^2]\\ &= E[(\Im\{d(n)\} - \Im\{\mathbf{w}_{\text{ci}}^H(n)\mathbf{x}_u(n)\})^2]\end{aligned} \tag{23}$$

and its minimisation can be recursively performed based on the conjugate derivative $\nabla J_i(n) = \partial J_i(n)/\partial \mathbf{w}_{\text{ci}}^*(n)$, to update its weight $\mathbf{w}_{\text{ci}}(n)$ as

$$\text{NCLMSi}: \quad \mathbf{w}_{\text{ci}}(n+1) = \mathbf{w}_{\text{ci}}(n) + j\mu\Im\{e_{\text{ci}}(n)\}\mathbf{x}_u(n) \tag{24}$$

where

$$e_{\text{ci}}(n) = d(n) - \mathbf{w}_{\text{ci}}^H(n)\mathbf{x}_u(n) \tag{25}$$

By combining together the real part of the output of NCLMSr and the imaginary part of the output of NCLMSi, the instantaneous output of the proposed DC-NCLMS is obtained as

$$\text{DC}-\text{NCLMS}: \quad e(n) = \Re\{e_{\text{cr}}(n)\} + j\Im\{e_{\text{ci}}(n)\} \tag{26}$$

Remark 2. The proposed DC-NCLMS based SI canceller is obtained by minimising the cost functions $J_r(n)$ and $J_i(n)$ in (12) separately but simultaneously. Upon comparing (18) with (22), and (14) with (25), we observe that the complex-valued output error $e(n)$ of ANCLMS is made up of the real part of the NCLMSr output $e_{\text{cr}}(n)$, that is, $\Re\{e_{\text{cr}}(n)\}$, and the imaginary part of the NCLMSi output $e_{\text{ci}}(n)$, that is, $\Im\{e_{\text{ci}}(n)\}$. Note that both $e_{\text{cr}}(n)$ and $e_{\text{ci}}(n)$ are also complex-valued and different from $e(n)$ in (10). Although the proposed DC-NCLMS exhibits a similar form to that of DC-CLMS [29], its input $\mathbf{x}_u(n)$ is now a nonlinear augmented regressor due to the presence of the nonlinear SI components $\mathbf{x}_{\text{IMD}}(n)$ and $\mathbf{x}_{\text{IMD}}^*(n)$.

4. Performance analysis of the proposed DC-NCLMS based SI canceller

In this section, we provide a comprehensive mean and mean square convergence analyses of the proposed DC-NCLMS based SI canceller for FD DCTs in the presence of major circuit imperfections, such as frequency-dependent Tx and Rx I/Q imbalance, PA nonlinearity, thermal noise and quantisation noise. A unified framework to theoretically quantify its SI cancellation capabilities in both the transient and steady state stages is also provided.

4.1. Mean convergence analysis

Based on (21) and (24), the two $(M+N)\times 1$ weight error vectors of DC-NCLMS are given by [40,41]

$$\widetilde{\mathbf{w}}_{\text{cr}}(n) = \mathbf{w}_{\text{cr}}(n) - \mathbf{w}_{\text{cr}}^{\text{o}} \tag{27}$$

and

$$\widetilde{\mathbf{w}}_{\text{ci}}(n) = \mathbf{w}_{\text{ci}}(n) - \mathbf{w}_{\text{ci}}^{\text{o}} \tag{28}$$

so that the real part of the filter output error within NCLMSr, that is, $\Re[e_{\text{cr}}(n)]$ in (22), becomes

$$\Re\{e_{\text{cr}}(n)\} = \Re\{v(n) + q(n)\} - \Re\{\widetilde{\mathbf{w}}_{\text{cr}}^H(n)\mathbf{x}_u(n)\} \tag{29}$$

In a similar way, from (25), we have

$$\Im\{e_{\text{ci}}(n)\} = \Im\{v(n) + q(n)\} - \Im\{\widetilde{\mathbf{w}}_{\text{ci}}^H(n)\mathbf{x}_u(n)\} \tag{30}$$

Now, upon substituting (27) and (29) into (21), the weight error update in NCLMSr becomes

$$\begin{aligned}\widetilde{\mathbf{w}}_{\text{cr}}(n+1) &= \left(\mathbf{I}_{M+N} - \frac{1}{2}\mu\mathbf{x}_u(n)\mathbf{x}_u^H(n)\right)\widetilde{\mathbf{w}}_{\text{cr}}(n)\\ &\quad - \frac{1}{2}\mu\mathbf{x}_u(n)\mathbf{x}_u^T(n)\widetilde{\mathbf{w}}_{\text{cr}}^*(n) + \mu\Re\{v(n)+q(n)\}\mathbf{x}_u(n)\end{aligned} \tag{31}$$

Similarly, by taking (28) and (30) into (24), we have

$$\widetilde{\mathbf{w}}_{\mathrm{ci}}(n+1)=\left(\mathbf{I}_{M+N}-\frac{1}{2}\mu\mathbf{x}_u(n)\mathbf{x}_u^H(n)\right)\widetilde{\mathbf{w}}_{\mathrm{ci}}(n)+\frac{1}{2}\mu\mathbf{x}_u(n)\mathbf{x}_u^T(n)\widetilde{\mathbf{w}}_{\mathrm{ci}}^*(n)+j\mu\Im\{v(n)+q(n)\}\mathbf{x}_u(n) \quad (32)$$

Upon applying the statistical expectation operator, $E[\cdot]$, to both sides of (31), and considering the statistical independence among $v(n)$, $q(n)$ and $\mathbf{x}_u(n)$ [42,43], the evolution of $\widetilde{\mathbf{w}}_{\mathrm{cr}}(n+1)$ is governed by

$$E[\widetilde{\mathbf{w}}_{\mathrm{cr}}(n+1)]=\left(\mathbf{I}_{M+N}-\frac{1}{2}\mu\mathbf{R}_u\right)E[\widetilde{\mathbf{w}}_{\mathrm{cr}}(n)] \quad (33)$$

where $\mathbf{R}_u=E[\mathbf{x}_u(n)\mathbf{x}_u^H(n)]$ is the input covariance matrix, which, according to (5), can be further expanded as

$$\mathbf{R}_u=E[\mathbf{x}_u(n)\mathbf{x}_u^H(n)]=\begin{bmatrix}\sigma_x^2\mathbf{I}_M & \mathbf{\Omega}^T\\ \mathbf{\Omega} & 6k_{\mathrm{TIQ}}^3\sigma_x^6\mathbf{I}_N\end{bmatrix} \quad (34)$$

Next, using the Gaussian fourth order moment factorising theorem, matrix $\mathbf{\Omega}$ can be further evaluated as

$$\mathbf{\Omega}=\begin{bmatrix}E[\mathbf{x}_d(n)\mathbf{x}_{\mathrm{IMD}}^H(n)] & \mathbf{0}_{N\times(M-N)}\end{bmatrix}=\begin{bmatrix}2k_{\mathrm{TIQ}}^{3/2}\sigma_x^4\mathbf{I}_N & \mathbf{0}_{N\times(M-N)}\end{bmatrix}$$

where $\mathbf{x}_d(n)=[x(n),x(n-1),\ldots,x(n-N+1)]^T$ consists of the first N elements of the SI vector $\mathbf{x}(n)$.

In a similar way, for the NCLMSi process, we have

$$E[\widetilde{\mathbf{w}}_{\mathrm{ci}}(n+1)]=\left(\mathbf{I}_{M+N}-\frac{1}{2}\mu\mathbf{R}_u\right)E[\widetilde{\mathbf{w}}_{\mathrm{ci}}(n)] \quad (35)$$

Observe from (33) and (35) that both the real and imaginary channels share an identical transition matrix in their weight error vector evolution. Therefore, the unified bound on the step-size μ to guarantee the mean convergence of the proposed DC-NCLMS stems from [40]

$$\left|1-\frac{1}{2}\mu\lambda_k\right|<1 \qquad k=1,\ldots,M+N \quad (36)$$

where λ_k is the kth eigenvalue of $\mathbf{R}_u$.

On the other hand, by applying the standard eigenvalue decomposition to $\mathbf{R}_u$, we have

$$\mathbf{R}_u=\mathbf{U}\mathbf{\Lambda}\mathbf{U}^H \quad (37)$$

where $\mathbf{U}$ is a unitary matrix, and $\mathbf{\Lambda}$ is a diagonal matrix composed of the eigenvalues of $\mathbf{R}_u$.

By further solving $\det[\mathbf{R}_u-\lambda\mathbf{I}_{M+N}]=0$, and after a few algebraic manipulations, we arrive at

$$\begin{aligned}\lambda_1&=E[|x(n)|^2]=\sigma_x^2\\ \lambda_{2,3}&=\frac{1}{2}\left\{E[|x(n)|^2]+k_{\mathrm{TIQ}}^3E[|x(n)|^6]\right.\\ &\left.\pm\sqrt{\left(E[|x(n)|^2]+k_{\mathrm{TIQ}}^3E[|x(n)|^6]\right)^2-k_{\mathrm{TIQ}}^3\left(E[|x(n)|^4]\right)^2}\right\}\\ &=\frac{\sigma_x^2+6k_{\mathrm{TIQ}}^3\sigma_x^6\pm\sigma_x^2\sqrt{1-2k_{\mathrm{TIQ}}^3\sigma_x^4+36k_{\mathrm{TIQ}}^6\sigma_x^8}}{2}\end{aligned} \quad (38)$$

where the algebraic multiplicities of λ_1, λ_2 and λ_3 are respectively $(M-N)$, N and N. Since it is easy to verify that $\lambda_2>\lambda_1>\lambda_3>0$, the bound on the step-size μ which preserves the mean stability of the proposed DC-NCLMS based SI canceller, now becomes

$$0<\mu<\frac{4}{\lambda_{\max}[\mathbf{R}^b]}=\frac{4}{\sigma_x^2+6k_{\mathrm{TIQ}}^3\sigma_x^6+\sigma_x^2\sqrt{1-2k_{\mathrm{TIQ}}^3\sigma_x^4+36k_{\mathrm{TIQ}}^6\sigma_x^8}} \quad (39)$$

Remark 3. The upper bound on the step-size μ of the proposed DC-NCLMS based SI canceller is exactly twice that of its ANCLMS counterpart [28], implying that DC-NCLMS theoretically converges twice as fast as ANCLMS. It is also worth noticing that the eigenvalues of the covariance matrix $\mathbf{R}_u$ are the same as those of the input covariance matrix of ANCLMS, but with halved algebraic multiplicities. This is because the input SI vector $\mathbf{x}_u(n)$ of DC-NCLMS, defined in (5), is of half the length of its augmented counterpart $\mathbf{x}_b(n)$ within ANCLMS in (7).

4.2. Mean square convergence analysis

From (26), the MSE $J(n)$ of DC-NCLMS can be further evaluated as

$$J(n)=E[|e(n)|^2]=\underbrace{E[(\Re\{e_{\mathrm{cr}}(n)\})^2]}_{J_{\mathrm{cr}}(n)}+\underbrace{E[(\Im\{e_{\mathrm{ci}}(n)\})^2]}_{J_{\mathrm{ci}}(n)} \quad (40)$$

By using the standard independence assumptions, $J_{\mathrm{cr}}(n)$ and $J_{\mathrm{ci}}(n)$, we next arrive at

$$\begin{aligned}J_{\mathrm{cr}}(n)&=E\left[\left(\Re\{v(n)+q(n)-\widetilde{\mathbf{w}}_{\mathrm{cr}}^H(n)\mathbf{x}_u(n)\}\right)^2\right]\\ &=\frac{1}{2}\sigma_v^2+\frac{1}{2}\sigma_q^2+\frac{1}{4}E\left[\left(\widetilde{\mathbf{w}}_{\mathrm{cr}}^H(n)\mathbf{x}_u(n)+\widetilde{\mathbf{w}}_{\mathrm{cr}}^T(n)\mathbf{x}_u^*(n)\right)^2\right]\\ &=\frac{1}{2}\sigma_v^2+\frac{1}{2}\sigma_q^2+\frac{1}{4}E\left[\widetilde{\mathbf{w}}_{\mathrm{cr}}^H(n)\mathbf{x}_u(n)\mathbf{x}_u^H(n)\widetilde{\mathbf{w}}_{\mathrm{cr}}(n)\right.\\ &\left.+\widetilde{\mathbf{w}}_{\mathrm{cr}}^T(n)\mathbf{x}_u^*(n)\mathbf{x}_u^T(n)\widetilde{\mathbf{w}}_{\mathrm{cr}}^*(n)\right]\\ &=\frac{1}{2}\sigma_v^2+\frac{1}{2}\sigma_q^2+\frac{1}{4}\mathrm{Tr}\left\{\mathbf{R}_u[\mathbf{K}_{\mathrm{cr}}(n)+\mathbf{K}_{\mathrm{cr}}^*(n)]\right\}\end{aligned} \quad (41)$$

and

$$\begin{aligned}J_{\mathrm{ci}}(n)&=E\left[\left(\Im\{v(n)+q(n)-\widetilde{\mathbf{w}}_{\mathrm{ci}}^H(n)\mathbf{x}_u(n)\}\right)^2\right]\\ &=\frac{1}{2}\sigma_v^2+\frac{1}{2}\sigma_q^2+\frac{1}{4}E\left[\left(\widetilde{\mathbf{w}}_{\mathrm{ci}}^H(n)\mathbf{x}_u(n)+\widetilde{\mathbf{w}}_{\mathrm{ci}}^T(n)\mathbf{x}_u^*(n)\right)^2\right]\\ &=\frac{1}{2}\sigma_v^2+\frac{1}{2}\sigma_q^2+\frac{1}{4}E\left[\widetilde{\mathbf{w}}_{\mathrm{ci}}^H(n)\mathbf{x}_u(n)\mathbf{x}_u^H(n)\widetilde{\mathbf{w}}_{\mathrm{ci}}(n)\right.\\ &\left.+\widetilde{\mathbf{w}}_{\mathrm{ci}}^T(n)\mathbf{x}_u^*(n)\mathbf{x}_u^T(n)\widetilde{\mathbf{w}}_{\mathrm{ci}}^*(n)\right]\\ &=\frac{1}{2}\sigma_v^2+\frac{1}{2}\sigma_q^2+\frac{1}{4}\mathrm{Tr}\left\{\mathbf{R}_u[\mathbf{K}_{\mathrm{ci}}(n)+\mathbf{K}_{\mathrm{ci}}^*(n)]\right\}\end{aligned} \quad (42)$$

where $\mathbf{K}_{\mathrm{cr}}(n)=E[\widetilde{\mathbf{w}}_{\mathrm{cr}}(n)\widetilde{\mathbf{w}}_{\mathrm{cr}}^H(n)]$ and $\mathbf{K}_{\mathrm{ci}}(n)=E[\widetilde{\mathbf{w}}_{\mathrm{ci}}(n)\widetilde{\mathbf{w}}_{\mathrm{ci}}^H(n)]$ are the respective covariance matrices of the weight error vectors $\widetilde{\mathbf{w}}_{\mathrm{cr}}(n)$ and $\widetilde{\mathbf{w}}_{\mathrm{ci}}(n)$. Therefore, the MSE of DC-NCLMS in (40) can now be expressed as

$$J(n)=\sigma_v^2+\sigma_q^2+\frac{1}{4}\mathrm{Tr}\left\{\mathbf{R}_u[\mathbf{K}_{\mathrm{cr}}(n)+\mathbf{K}_{\mathrm{cr}}^*(n)+\mathbf{K}_{\mathrm{ci}}(n)+\mathbf{K}_{\mathrm{ci}}^*(n)]\right\} \quad (43)$$

The convergence behaviour of $J(n)$ follows from that of $\mathbf{K}_{\mathrm{cr}}(n)$ and $\mathbf{K}_{\mathrm{ci}}(n)$, as well as their conjugates. We shall first consider convergence of the NCLMSr, which can be evaluated by applying the Hermitian transpose operator $(\cdot)^H$ to both sides of (31), to give

$$\widetilde{\mathbf{w}}_{\mathrm{cr}}^H(n+1)=\widetilde{\mathbf{w}}_{\mathrm{cr}}^H(n)\left(\mathbf{I}_{M+N}-\frac{1}{2}\mu\mathbf{x}_u(n)\mathbf{x}_u^H(n)\right)-\frac{1}{2}\mu\widetilde{\mathbf{w}}_{\mathrm{cr}}^T(n)\mathbf{x}_u^*(n)\mathbf{x}_u^H(n)+\mu\mathbf{x}_u^H(n)\Re\{v(n)+q(n)\} \quad (44)$$

Upon multiplying both sides of (44) with (31), and applying again the statistical expectation operator $E[\cdot]$ and the standard independence assumptions, we have

$$\mathbf{K}_{\mathrm{cr}}(n+1)=\mathbf{I}_{M+N}-\frac{1}{2}\mu\mathbf{R}_u\mathbf{K}_{\mathrm{cr}}(n)-\frac{1}{2}\mu\mathbf{K}_{\mathrm{cr}}(n)\mathbf{R}_u+\frac{1}{4}\mu^2E[\mathbf{x}_u(n)\mathbf{x}_u^H(n)\widetilde{\mathbf{w}}_{\mathrm{cr}}(n)\widetilde{\mathbf{w}}_{\mathrm{cr}}^H(n)\mathbf{x}_u(n)\mathbf{x}_u^H(n)]$$

$$+\frac{1}{4}\mu^2 E[\mathbf{x}_u(n)\mathbf{x}_u^T(n)\widetilde{\mathbf{w}}_{\mathrm{cr}}^*(n)\widetilde{\mathbf{w}}_{\mathrm{cr}}^T(n)\mathbf{x}_u^*(n)\mathbf{x}_u^H(n)]$$
$$+\frac{1}{2}\mu^2(\sigma_v^2+\sigma_q^2)\mathbf{R}_u \tag{45}$$

Remark 4. Since $\mathbf{x}_u(n)$ contains higher-order moments which are non-Gaussian, the conventional Gaussian fourth order moment factorising theorem used in [26,43] is no longer applicable to evaluate the fourth and fifth terms of the right hand side of (45). We therefore resort to matrix vectorisation instead of matrix diagonalisation to evaluate the mean square convergence behaviour of NCLMSr [44].

The following matrix vectorisation lemma for arbitrary matrices {**A, B, C**} [44]

$$\mathrm{vec}\{\mathbf{ABC}\} = (\mathbf{C}^T \otimes \mathbf{A})\mathrm{vec}\{\mathbf{B}\}$$

applied to Eq. (45) now yields a recursion for the vector $\mathrm{vec}\{\mathbf{K}_{\mathrm{cr}}(n)\}$ in the form

$$\mathrm{vec}\{\mathbf{K}_{\mathrm{cr}}(n+1)\} = \left(\mathbf{I}_{M+N} - \frac{1}{2}\mu\mathbf{S} + \frac{1}{4}\mu^2\mathbf{T}_1\right)\mathrm{vec}\{\mathbf{K}_{\mathrm{cr}}(n)\} + \frac{1}{4}\mu^2\mathbf{T}_2\mathrm{vec}\{\mathbf{K}_{\mathrm{cr}}^*(n)\} + \frac{1}{2}\mu^2(\sigma_v^2+\sigma_q^2)\mathrm{vec}\{\mathbf{R}_u\} \tag{46}$$

where

$$\mathbf{S} = \mathbf{I}_{M+N}\otimes\mathbf{R}_u + \mathbf{R}_u\otimes\mathbf{I}_{M+N} \tag{47}$$

$$\mathbf{T}_1 = E\left[\left(\mathbf{x}(n)\mathbf{x}_u^H(n)\right)\otimes\left(\mathbf{x}_u(n)\mathbf{x}_u^H(n)\right)\right] \tag{48}$$

$$\mathbf{T}_2 = E\left[\left(\mathbf{x}(n)\mathbf{x}_u^T(n)\right)\otimes\left(\mathbf{x}_u^*(n)\mathbf{x}_u^H(n)\right)\right] \tag{49}$$

Observe from (46) that both $\mathrm{vec}\{\mathbf{K}_{\mathrm{cr}}(n)\}$ and its conjugate $\mathrm{vec}\{\mathbf{K}_{\mathrm{cr}}^*(n)\}$ are now involved, and are concatenated to form an augmented column vector $\boldsymbol{\kappa}_{\mathrm{cr}}(n)$, given by

$$\boldsymbol{\kappa}_{\mathrm{cr}}(n) = \left[(\mathrm{vec}\{\mathbf{K}_{\mathrm{cr}}(n)\})^T, (\mathrm{vec}\{\mathbf{K}_{\mathrm{cr}}(n)\})^H\right]^T \tag{50}$$

By considering both the expression in (46) and its complex conjugate, we arrive at

$$\boldsymbol{\kappa}_{\mathrm{cr}}(n+1) = \underbrace{\left(\mathbf{I}_{2M+2N} - \frac{1}{2}\mu\mathbb{S} + \frac{1}{4}\mu^2\mathbb{T}\right)}_{\mathbf{F}_{\mathrm{cr}}}\boldsymbol{\kappa}_{\mathrm{cr}}(n) + \frac{1}{2}\mu^2(\sigma_v^2+\sigma_q^2)\boldsymbol{r}_u \tag{51}$$

where

$$\mathbb{S} = \begin{bmatrix}\mathbf{S} & \mathbf{0}\\ \mathbf{0} & \mathbf{S}\end{bmatrix}$$

$$\mathbb{T} = \begin{bmatrix}\mathbf{T}_1 & \mathbf{T}_2\\ \mathbf{T}_2 & \mathbf{T}_1\end{bmatrix}$$

and

$$\boldsymbol{r}_u = \left[(\mathrm{vec}\{\mathbf{R}_u\})^T, (\mathrm{vec}\{\mathbf{R}_u\})^H\right]^T \tag{52}$$

The condition on the step-size μ to guarantee the mean square stability of the NCLMSr channel now follows from $|\lambda_{\max}[\mathbf{F}_{\mathrm{cr}}]| < 1$. According to the analysis in [44], for positive definite matrices $\mathbf{R}_u$ and $\mathbb{S}$, and a nonnegative definite matrix $\mathbb{T}$, this condition is valid as long as μ satisfies

$$0 < \mu < \mu_{\max} = \min\left\{\frac{1}{\lambda_{\max}[\mathbb{S}^{-1}\mathbb{T}]}, \frac{1}{\lambda_{\max}[\mathbb{L}]}\right\} \tag{53}$$

where

$$\mathbb{L} = \begin{bmatrix}\frac{\mathbb{S}}{2} & -\frac{\mathbb{T}}{2}\\ \mathbf{I}_{(2M+2N)^2} & \mathbf{0}\end{bmatrix} \tag{54}$$

On the other hand, within the NCLMSi channel, upon applying the Hermitian operator $(\cdot)^H$ to both sides of (32), we have

$$\widetilde{\mathbf{w}}_{\mathrm{ci}}^H(n+1) = \widetilde{\mathbf{w}}_{\mathrm{ci}}^H(n)\left(\mathbf{I}_{M+N} - \frac{1}{2}\mu\mathbf{x}_u(n)\mathbf{x}_u^H(n)\right) - \widetilde{\mathbf{w}}_{\mathrm{ci}}^T(n)\frac{1}{2}\mu\mathbf{x}_u^*(n)\mathbf{x}_u^H(n) + \mu\mathbf{x}_u^H(n)\Re\{v(n)+q(n)\} \tag{55}$$

In a similar way, by multiplying both sides of (32) with (55) and taking the statistical expectation $E[\cdot]$, the evolution of the weight error covariance matrix of NCLMSi, that is, $\mathbf{K}_{\mathrm{ci}}(n)$, can be analysed from

$$\mathbf{K}_{\mathrm{ci}}(n+1) = \mathbf{I}_{M+N} - \frac{1}{2}\mu\mathbf{R}_u\mathbf{K}_{\mathrm{ci}}(n) - \frac{1}{2}\mu\mathbf{K}_{\mathrm{ci}}(n)\mathbf{R}_u + \frac{1}{4}\mu^2 E[\mathbf{x}_u(n)\mathbf{x}_u^H(n)\widetilde{\mathbf{w}}_{\mathrm{ci}}(n)\widetilde{\mathbf{w}}_{\mathrm{ci}}^H(n)\mathbf{x}_u(n)\mathbf{x}_u^H(n)] + \frac{1}{4}\mu^2 E[\mathbf{x}_u(n)\mathbf{x}_u^T(n)\widetilde{\mathbf{w}}_{\mathrm{ci}}^*(n)\widetilde{\mathbf{w}}_{\mathrm{ci}}^T(n)\mathbf{x}_u^*(n)\mathbf{x}_u^H(n)] + \frac{1}{2}\mu^2(\sigma_v^2+\sigma_q^2)\mathbf{R}_u \tag{56}$$

Remark 5. Observe that $\mathbf{K}_{\mathrm{ci}}(n)$ in (56) now shares the same recursion form as $\mathbf{K}_{\mathrm{cr}}(n)$ in (45), which indicates that the only difference between $\mathbf{K}_{\mathrm{cr}}(n)$ and $\mathbf{K}_{\mathrm{ci}}(n)$ stems from their initialisations $\mathbf{K}_{\mathrm{cr}}(0)$ and $\mathbf{K}_{\mathrm{ci}}(0)$. Therefore, the condition on the step-size μ to ensure the mean-square stability of the NCLMSi channel is the same as that of its NCLMSr counterpart in (53). In other words, the mean square convergence of the proposed DC-NCLMS based SI canceller is guaranteed if the step-size μ satisfies (53).

4.3. Steady state analysis

After choosing a step-size μ according to the range in (53), when $n\to\infty$, the steady state MSE, $J(\infty)$, can be evaluated from (40) as [45,46]

$$J(\infty) = J_{\mathrm{cr}}(\infty) + J_{\mathrm{ci}}(\infty) = \sigma_v^2 + \sigma_q^2 + \frac{1}{4}\mathrm{Tr}\left\{\mathbf{R}_u[\mathbf{K}_{\mathrm{cr}}(\infty) + \mathbf{K}_{\mathrm{cr}}^*(\infty) + \mathbf{K}_{\mathrm{ci}}(\infty) + \mathbf{K}_{\mathrm{ci}}^*(\infty)]\right\} \tag{57}$$

From (51), the steady state value of $\boldsymbol{\kappa}_{\mathrm{cr}}(n)$ is given by

$$\boldsymbol{\kappa}_{\mathrm{cr}}(\infty) = \frac{1}{2}\mu^2(\sigma_v^2+\sigma_q^2)(\mathbf{I}_{2M+2N} - \mathbf{F}_{\mathrm{cr}})^{-1}\boldsymbol{r}_u \tag{58}$$

Recall from (50) that, $\mathrm{vec}\{\mathbf{K}_{\mathrm{cr}}(\infty)\}$ is the first half of the entries of $\boldsymbol{\kappa}_{\mathrm{cr}}(\infty)$, so that

$$\mathbf{K}_{\mathrm{cr}}(\infty) = \mathrm{vec}^{-1}\{\boldsymbol{\kappa}_{\mathrm{cr1}}(\infty)\} \tag{59}$$

where $\boldsymbol{\kappa}_{\mathrm{cr1}}(\infty)$ is a column vector composed by the first half of the entries of $\boldsymbol{\kappa}_{\mathrm{cr}}(\infty)$. Also note that according to Remark 5, the convergence of $\mathbf{K}_{\mathrm{cr}}(n)$ and $\mathbf{K}_{\mathrm{ci}}(n)$ differs only in their initialisations, so that at the steady state, $\mathbf{K}_{\mathrm{cr}}(\infty) = \mathbf{K}_{\mathrm{ci}}(\infty)$. Keeping this in mind and upon inserting (59) into (57), we have

$$J(\infty) = \sigma_v^2 + \sigma_q^2 + \mathrm{Tr}\left\{\mathbf{R}_u\Re\left\{\mathrm{vec}^{-1}\{\boldsymbol{\kappa}_{\mathrm{cr1}}(\infty)\}\right\}\right\} \tag{60}$$

To find a more analytically interpretable expression for $J(\infty)$, first observe that matrices $\mathbf{T}_1$ and $\mathbf{T}_2$ in (46) are multiplied by μ^2, so that it is reasonable to omit these terms for a sufficiently small step-size μ. With that, considering the standard eigenvalue decomposition of $\mathbf{R}_u$ in (37), from (45), we now have

$$\widetilde{\mathbf{K}}_{\mathrm{cr}}(n+1) = \widetilde{\mathbf{K}}_{\mathrm{cr}}(n) + \frac{1}{2}\mu^2(\sigma_v^2+\sigma_q^2)\boldsymbol{\Lambda} - \frac{1}{2}\mu\boldsymbol{\Lambda}\widetilde{\mathbf{K}}_{\mathrm{cr}}(n) - \frac{1}{2}\mu\widetilde{\mathbf{K}}_{\mathrm{cr}}(n)\boldsymbol{\Lambda} \tag{61}$$

where $\widetilde{\mathbf{K}}_{\mathrm{cr}}(n) = \mathbf{U}^H\mathbf{K}_{\mathrm{cr}}(n)\mathbf{U}$, and when $n\to\infty$, this yields

$$\widetilde{\mathbf{K}}_{\mathrm{cr}}(\infty) = \frac{1}{2}\mu(\sigma_v^2+\sigma_q^2)\mathbf{I}_{M+N} \tag{62}$$

Since $\widetilde{\mathbf{K}}_{\text{cr}}(\infty)$ is real-valued and $\widetilde{\mathbf{K}}_{\text{ci}}(\infty)=\widetilde{\mathbf{K}}_{\text{cr}}(\infty)$, the steady state MSE $J(\infty)$ in (57) can now be approximated by

$$\begin{aligned}J_{\text{ap}}(\infty)&=\sigma_v^2+\sigma_q^2+\text{Tr}\{\mathbf{U}\mathbf{\Lambda}\widetilde{\mathbf{K}}_{\text{cr}}(\infty)\mathbf{U}^H\}\\&=\sigma_v^2+\sigma_q^2+\frac{\mu(\sigma_v^2+\sigma_q^2)\text{Tr}\{\mathbf{\Lambda}\}}{2}\\&=(\sigma_v^2+\sigma_q^2)\left[\mu\left(\frac{M\sigma_x^2}{2}+3Nk_{\text{TIQ}}^3\sigma_x^6\right)+1\right]\end{aligned}\tag{63}$$

By definition, the steady state MSE of the LMS-based adaptive algorithm is described by [47]

$$J(\infty)=J_{\min}+J_{\text{ex}}(\infty)\tag{64}$$

where in our case

$$J_{\min}=\sigma_v^2+\sigma_q^2\tag{65}$$

and $J_{\text{ex}}(\infty)$ is the steady state excess MSE (EMSE), which can be obtained from (63) as

$$J_{\text{ex,DC-NCLMS}}(\infty)=\mu(\sigma_v^2+\sigma_q^2)\left(\frac{M\sigma_x^2}{2}+3Nk_{\text{TIQ}}^3\sigma_x^6\right)\tag{66}$$

For comparison, the steady state EMSE of ANCLMS is given by [28]

$$J_{\text{ex,ANCLMS}}(\infty)=\mu(\sigma_v^2+\sigma_q^2)(M\sigma_x^2+6Nk_{\text{TIQ}}^3\sigma_x^6)\tag{67}$$

Remark 6. From (66) and (67), observe that for the same step-size, μ, the steady state EMSE of the proposed DC-NCLMS is half that of ANCLMS. This conforms with the analysis in *Remark 3* that ANCLMS converges twice as fast as DC-NCLMS. In other words, to ensure equivalent transient and steady state performance between DC-NCLMS and ANCLMS, the step-size μ chosen for DC-NCLMS should be twice that of ANCLMS [31].

5. Further convergence speed improvement of the proposed DC-NCLMS SI canceller

In the presence of the third-order intermodulation SI components in $\mathbf{x}_u(n)$, LMS-like adaptive filters are subject to slow convergence due to the large condition number of $\mathbf{R}_u$ [48]. In the literature, there are several approaches to enhance the convergence speed of adaptive SI cancellers [28,49]. In this section, to address this issue, two variants of the DC-NCLMS based SI canceller are introduced, which are respectively named as the dual-channel nonlinear complex affine projection (DC-NCAP) and the data prewhitening assisted DC-NCLMS (DPA-DC-NCLMS).

5.1. DC-NCAP Based SI canceller

Compared to other established adaptive filtering algorithms, such as normalised LMS and recursive least squares, the affine projection algorithm exploits the affine subspace projections to update the weight vector on the basis of both past and current input vectors, and in this way exhibits a desirable trade-off between the computational complexity and the convergence rate. The augmented AP algorithm for the processing of both circular and non-circular signals was proposed in [49]. Inspired by this approach, we again make use of the duality between the complex and real domain in the affine subspace, to introduce the DC-NCAP based SI canceller. Based on the dual-channel SI cancellation model in (17), the vector of observed signals, $\mathbf{d}(n)$, from K most recent observations, can be represented as

$$\mathbf{d}(n)=\Re\{\mathbf{X}_u^H(n)\mathbf{w}_{\text{cra}}(n)\}+j\Im\{\mathbf{X}_u^H(n)\mathbf{w}_{\text{cia}}(n)\}+\mathbf{v}(n)+\mathbf{q}(n)\tag{68}$$

where $\mathbf{d}_u(n)=[d(n-K+1),\ldots,d(n)]^T$ is the $K\times 1$ vector of observed signals, $\mathbf{X}_u(n)=[\mathbf{x}_u(n-K+1),\ldots,\mathbf{x}_u(n)]^T$ is the $(M+N)\times K$ matrix in the filter memory, $\mathbf{w}_{\text{cra}}(n)$ and $\mathbf{w}_{\text{cia}}(n)$ are the two weight vectors in the DC-NCAP canceller which track the corresponding system coefficients, $\mathbf{w}_{\text{cr}}^o$ and $\mathbf{w}_{\text{ci}}^o$, while $\mathbf{v}(n)=[v(n-K+1),\ldots,v(n)]^T$ and $\mathbf{q}(n)=[q(n-K+1),\ldots,q(n)]^T$ respectively represent the $K\times 1$ thermal noise and quantisation noise vectors. The proposed DC-NCAP SI canceller is then formed by splitting its MSE into two parts and performing two independent gradient descent weight update processes. Similar to the derivation of the DC-NCLMS in (21) - (26), the final weight update process of the proposed DC-NCAP is given by

$$\begin{aligned}\mathbf{w}_{\text{cra}}(n+1)=\mathbf{w}_{\text{cra}}(n)+\mu\mathbf{X}_u(n)\big(&\mathbf{X}_u^H(n)\mathbf{X}_u(n)+\mathbf{X}_u^T(n)\mathbf{X}_u^*(n)\\&+\delta\mathbf{I}\big)^{-1}\Re\{\mathbf{e}_{\text{cra}}(n)\}\end{aligned}\tag{69}$$

$$\mathbf{e}_{\text{cra}}(n)=\mathbf{d}(n)-\mathbf{X}_u^H(n)\mathbf{w}_{\text{cra}}(n)\tag{70}$$

$$\begin{aligned}\mathbf{w}_{\text{cia}}(n+1)=\mathbf{w}_{\text{cia}}(n)+\mu\mathbf{X}_u(n)\big(&\mathbf{X}_u^H(n)\mathbf{X}_u(n)\\&+\mathbf{X}_u^T(n)\mathbf{X}_u^*(n)+\delta\mathbf{I}\big)^{-1}\Im\{\mathbf{e}_{\text{cia}}(n)\}\end{aligned}\tag{71}$$

$$\mathbf{e}_{\text{cia}}(n)=\mathbf{d}(n)-\mathbf{X}_u^H(n)\mathbf{w}_{\text{cia}}(n)\tag{72}$$

$$\mathbf{e}(n)=\Re\{\mathbf{e}_{\text{cra}}(n)\}+j\Im\{\mathbf{e}_{\text{cia}}(n)\}\tag{73}$$

where δ is a positive constant introduced to avoid singularities due to the inversion of a rank deficient matrix [31].

5.2. Data prewhitening assisted DC-NCLMS based SI canceller

Within the context of FD transceiver systems, the closed-form expression for $\mathbf{R}_u$ is readily available at the receiver. By virtue of this convenience, a data prewhitening scheme was proposed in [28] to stabilize the eigenvalue spread of the input covariance matrix of ANCLMS. Embarking upon this result, before performing the proposed DC-NCLMS digital SI cancellation, from the eigenvalue decomposition in (37) we can conduct a whitened input vector $\mathbf{x}_p(n)$ as

$$\mathbf{x}_p(n)=\mathbf{\Phi}\mathbf{x}_u(n)\tag{74}$$

where $\mathbf{\Phi}=[\mathbf{\Lambda}]^{-\frac{1}{2}}\mathbf{U}^H$. In this way, a data prewhitening assisted (DPA)-DC-NCLMS based SI canceller can be introduced as

$$\mathbf{w}_{\text{crp}}(n+1)=\mathbf{w}_{\text{crp}}(n)+\mu\Re\{e_{\text{crp}}(n)\}\mathbf{x}_p(n)\tag{75}$$

$$e_{\text{crp}}(n)=d(n)-\mathbf{w}_{\text{crp}}^H(n)\mathbf{x}_p(n)\tag{76}$$

$$\mathbf{w}_{\text{cip}}(n+1)=\mathbf{w}_{\text{cip}}(n)+j\mu\Im\{e_{\text{cip}}(n)\}\mathbf{x}_p(n)\tag{77}$$

$$e_{\text{cip}}(n)=d(n)-\mathbf{w}_{\text{cip}}^H(n)\mathbf{x}_p(n)\tag{78}$$

$$e(n)=\Re\{e_{\text{crp}}(n)\}+j\Im\{e_{\text{cip}}(n)\}\tag{79}$$

5.3. Computational complexity of the ANCLMS and the proposed SI cancellers

We next compare computational complexities of the original ANCLMS and the proposed dual channel based SI cancellers. Their

Table 1
Computational requirements per iteration of the considered SI cancellers, where M is the length of SI components and N the length of IMD SI components.

SI Canceller	Real Multiplications
ANCLMS [28]	$O\big(16(M+N)+2\big)$
DC-NCLMS	$O\big(8(M+N)+2\big)$
DPA-ANCLMS [28]	$O\big(16(M+N)^2+16(M+N)+2\big)$
DPA-DC-NCLMS	$O\big(4(M+N)^2+8(M+N)+2\big)$
DC-NCAP	$O\big(4K^2(M+N)^2+12K(M+N)+K^3+4K^2+4K\big)$

computational load is measured based on the number of real-valued multiplications required at each iteration[2], and is summarised in Table 1. Observe that the complex dual channel (CDC) processing framework requires roughly half of the load required by the original widely nonlinear processing framework. This is mainly because ANCLMS uses an augmented $(2M+2N)\times 1$ regressor vector, $\mathbf{x}_b(n)$, while DC-NCLMS uses a half-length regressor vector, $\mathbf{x}_u(n)$. This computational efficiency is more pronounced when the data prewhitening is employed, since the size of the whitening matrix $\mathbf{\Phi}$ in (74) is one quarter of its counterpart used for ANCLMS. The required multiplications of DC-NCAP largely depend on the matrix inversion operation in each iteration, as evidenced in (69) and (71), resulting in a much higher computational complexity than other schemes.

6. Simulations

Numerical examples were conducted in the MATLAB programming environment in order to evaluate the theoretical findings for the proposed DC-NCLMS based SI cancellers. The typical FD DCTs baseband equivalent channel impulse responses (CIRs) in (1) are given by [19]

$$\mathbf{h}^{\mathrm{o}} = \alpha_0\sqrt{k_{\mathrm{BB}}k_{\mathrm{LNA}}}f_{1,\mathrm{R}}(n)\star f_{1,\mathrm{T}}(n)\star f_{\mathrm{RFE}}(n) \tag{80}$$

$$\mathbf{g}^{\mathrm{o}} = \alpha_0\sqrt{k_{\mathrm{BB}}k_{\mathrm{LNA}}}\big(f_{1,\mathrm{R}}(n)\star f_{2,\mathrm{T}}(n)+f_{2,\mathrm{R}}(n)\star f^{*}_{1,\mathrm{T}}(n)\big)\star f^{*}_{\mathrm{RFE}}(n) \tag{81}$$

$$\mathbf{h}^{\mathrm{o}}_{\mathrm{IMD}} = \alpha_1\sqrt{k_{\mathrm{BB}}k_{\mathrm{LNA}}}f_{1,\mathrm{R}}(n)\star f_{\mathrm{RFE}}(n) \tag{82}$$

$$\mathbf{g}^{\mathrm{o}}_{\mathrm{IMD}} = \alpha_1\sqrt{k_{\mathrm{BB}}k_{\mathrm{LNA}}}f_{2,\mathrm{R}}(n)\star f^{*}_{\mathrm{RFE}}(n) \tag{83}$$

$$v(n) = \sqrt{k_{\mathrm{BB}}k_{\mathrm{LNA}}}f_{1,\mathrm{R}}(n)\star v_{\mathrm{th}}(n) \tag{84}$$

where the variable $f_{\mathrm{RFE}}(n)$ represents the residual effect of an imperfect analog SI cancellation procedure, involved in all the coefficients $\mathbf{h}^{\mathrm{o}}$, $\mathbf{g}^{\mathrm{o}}$, $\mathbf{h}^{\mathrm{o}}_{\mathrm{IMD}}$ and $\mathbf{g}^{\mathrm{o}}_{\mathrm{IMD}}$. In our simulations, $f_{\mathrm{RFE}}(n)$ was subject to a 3-tap static Rayleigh distribution justified in [17]. The considered FD DCT had a reasonable analog SI cancellation level at 45 dB. The variables $f_{1,\mathrm{T}}(n)$, $f_{2,\mathrm{T}}(n)$, $f_{1,\mathrm{R}}(n)$ and $f_{2,\mathrm{R}}(n)$ are respectively the frequency-dependent mixed CIRs for the direct and image channels in both the Tx and Rx within the FD DCT, all modeled as 2-tap static FIR filters [50]. As a result, the length of the end-to-end CIRs, $\mathbf{h}^{\mathrm{o}}$ and $\mathbf{g}^{\mathrm{o}}$, was $M=5$, while the length of the CIRs for the higher-order IMD SI components was $N=4$. The variable k_{BB} denotes the gain of the varying gain amplifier, for which the full description can be found in [28]. Other system parameters used in (80)-(84) are explained in Table 2. The power of quantisation noise $q(n)$, denoted by σ_q^2, is computed as [51]

$$\sigma_q^2 = \frac{p_{\mathrm{ADC}}}{10^{6.02\beta+4.76-\mathrm{PAPR}/10}} \tag{85}$$

Physical meanings of parameters p_{ADC}, β and PAPR are provided in Table 2. Throughout the simulations, the transmit SI signal, $x(n)$, and the received signal of interest, $x_{\mathrm{SOI}}(n)$, were both compliant with OFDM-based IEEE 802.11ac standards, and the key transmission parameters are listed in Table 3. Such a waveform conforms with the assumption made for the SI signal $x(n)$, i.e., it is a zero-mean proper Gaussian process.

Using typical system parameters in Table 2, a comparison of the powers of different signal components in a representative FD DCT is illustrated in Fig. 2. Observe that, apart from the original SI component, $\mathbf{x}(n)$, the image SI, $\mathbf{x}^{*}(n)$, which results from I/Q imbalance, was also dominant in the entire transmit power range. When the transmit power exceeded above 9 dBm, the IMD SI component, $\mathbf{x}_{\mathrm{IMD}}(n)$, which origins from PA distortion, became stronger

Table 2
System parameters in practical FD DCTs.

System parameters	Notation	Value
Receiver Sensitivity	p_{sen}	-89 dBm
SNR requirement	$\mathrm{SNR}_{\mathrm{req}}$	10 dB
Thermal noise floor	$\sigma^2_{v_{\mathrm{th}}}$	-104 dBm
Tx mixer gain	k_{TIQ}	6 dB
Rx mixer gain	k_{RIQ}	6 dB
Total RF attenuation	$\frac{\|\mathbf{h}^{\mathrm{o}}\|^2}{k_{\mathrm{TIQ}}k_{\mathrm{RIQ}}}$	45 dB
PA gain	α_0^2	25 dB
PA IIP3	α_0/α_1	18 dBm
LNA gain	k_{LNA}	25 dB
Dynamic range of ADC	p_{ADC}	7 dB
Peak-to-average-power ratio	PAPR	10 dB
ADC bits	β	12

Table 3
Parameters of the OFDM waveform used in simulations .

Parameter	Value
Constellation	QPSK
Number of carriers	64
Number of null carriers	14
Length of cyclic prefix	16
Bandwidth	20 MHz
OFDM symbol period	4 μs
Number of OFDM symbols	800
Oversampling factor	4

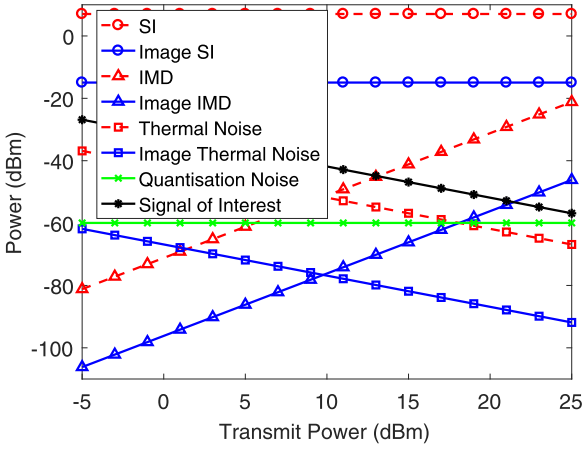

Fig. 2. Power comparison among different signal components in a representative FD transceiver, before digital SI cancellation and against different levels of transmit powers.

[2] One complex multiplication requires four real multiplications and two real additions. Since the covariance matrix, $\mathbf{R}_u$, is assumed to be known to the receiver, the computation of the matrix inversion operation in data prewhitening schemes is required in their initialisation only.

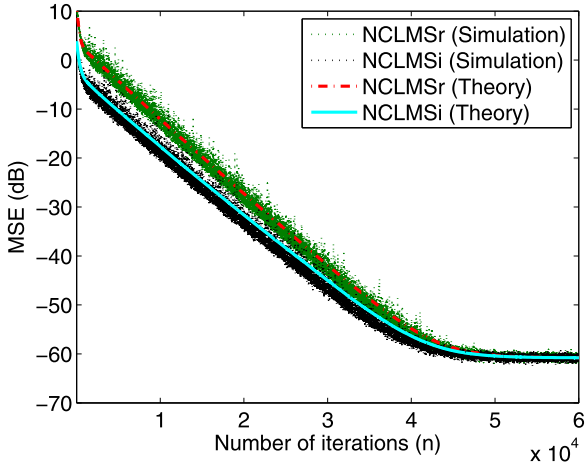

Fig. 3. Transient MSE performance of the real and imaginary branches, NCLMSr and NCLMSi, within DC-NCLMS. The transmit power of the considered FD DCT was set to 20 dBm.

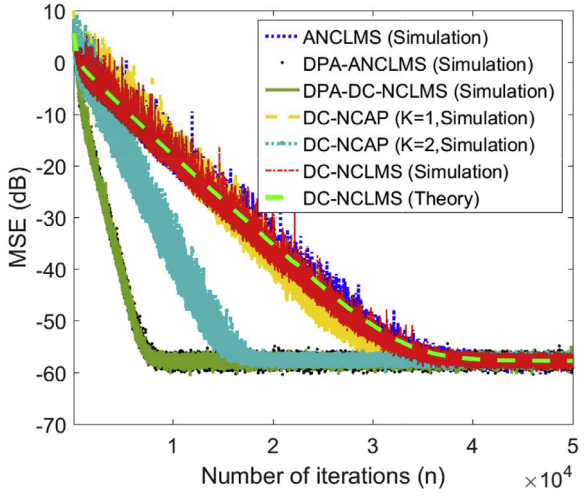

Fig. 4. Transient MSE performance of all the considered SI cancellers. The transmit power of the considered FD DCT was set to 20 dBm.

than the noise floor. Furthermore, the image IMD SI, $\mathbf{x}^*_{\text{IMD}}(n)$, a joint product of I/Q imbalance and PA distortion, linearly increased to become another major interference when the transmit power became even higher. These simulation results again motivate the need for the proposed DC-NCLMS canceller to simultaneously suppress the SI, image SI and IMD components, especially when the FD DCT operates in the high transmit power range.

Fig. 3 compares the theoretical and simulated transient MSE performance of the NCLMSr and NCLMSi channels within the proposed DC-NCLMS based SI canceller. The step-size μ was chosen to be $0.04\mu_{\text{MAX}}$, where μ_{MAX} is the upper bound which guarantees the mean square stability of DC-NCLMS, given in (53). The theoretical MSEs of NCLMSr and NCLMSi, that is, $J_{\text{cr}}(n)$ and $J_{\text{ci}}(n)$, were respectively evaluated using (41) and (42), with their weight error covariance matrices recursively obtained using (45) and (56). The theoretical results accurately demonstrated the desired properties of DC-NCLMS, although the NCLMSr and NCLMSi channels had different MSE initialisations, they arrived at the identical steady state MSE as that of ANCLMS. This is consistent with *Remark 6* because both channels share the same recursion form for the evolution of their respective weight error covariance matrices. Fig. 4compares the MSE evolution of all the considered SI cancellers. The step-size μ for ANCLMS, DC-NCLMS and DC-NCAP was respectively chosen as $0.05\mu_{\text{MAX}}$, $0.1\mu_{\text{MAX}}$ and $0.1\mu_{\text{MAX}}$, while for DPA-ANCLMS and DPA-DC-NCLMS, it was respectively set to 0.05 and 0.1. Several interesting observations can be drawn from Fig. 4. Firstly, an excellent agreement between the simulated MSE of the proposed DC-NCLMS and its theoretical evaluation in (43) can be observed in both the transient and steady state stages. Secondly, owing to the improvement on the condition number of the input covariance matrix, the data prewhitening scheme significantly accelerated the convergence of both ANCLMS and the proposed DC-NCLMS, and alleviated their performance discrepancy related to different independent initialisations in the transient stage. This is because a smaller eigenvalue spread within the input covariance matrix incurs a lower gradient noise. Thirdly, since DC-NCAP updates the weight vector on the basis of both past and current input vectors, it is expected to converge faster than DC-NCLMS, especially when the number of observations K becomes larger. This improvement is, however, achieved at the cost of a heavier computational burden, as discussed in Section 5.2, together with a higher steady state excess MSE (EMSE), as evidenced by quantitative results in Table 4. Finally, when the step-size μ in DC-NCLMS was set to be twice that of ANCLMS, those algorithms exhibited similar transient and steady state behaviour. The same situation was present when their data prewhitening schemes were employed. Besides, as discussed in *Remark 6*, when the original ANCLMS and the proposed DC-NCLMS SI cancellers employed the same step-size μ, the steady state excess MSE (EMSE) of DC-NCLMS was half that of ANCLMS. This phenomenon is further quantified by Table 4.

Table 4
Comparison of the steady state EMSEs of ANCLMS, DC-NCLMS and DC-NCAP. The transmit power of the considered FD DCT was set to 20 dB

Step-size μ	$0.05\mu_{\text{MAX}}$
ANCLMS (Simulation)	4.904×10^{-8}
ANCLMS (Theory)	4.810×10^{-8}
DC-NCLMS (Simulation)	2.402×10^{-8}
DC-NCLMS (Theory)	2.389×10^{-8}
DC-NCAP (K=1)	4.640×10^{-8}
DC-NCAP (K=2)	9.281×10^{-8}

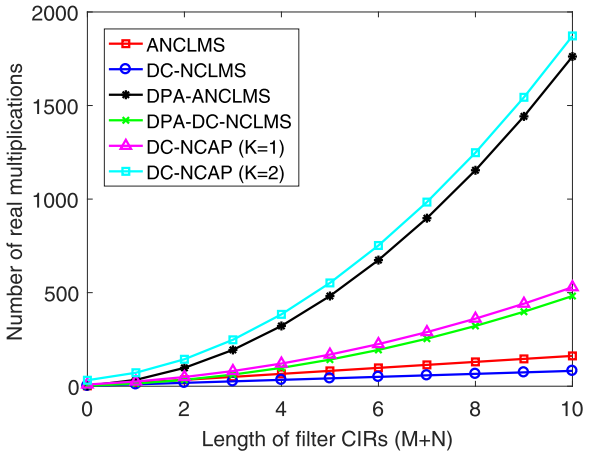

Fig. 5. Number of multiplications against the length of the CIRs.

While similar results produced by DC-NCLMS and ANCLMS have been observed in Fig. 4, the complex dual-channel (CDC) framework inherently requires lower computational burden, as discussed in Section 5.2. This is further illustrated in Fig. 5, where the computational requirements of all the considered SI cancellers are compared in terms of the number of real-valued multiplications per iteration. It can be observed that the numbers of multiplica-

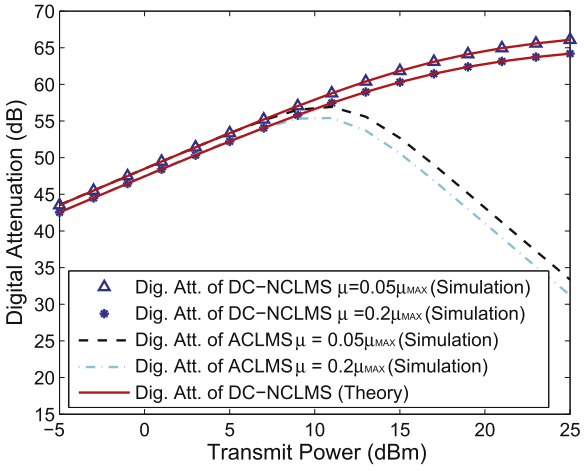

Fig. 6. Steady state performance of the proposed DC-NCLMS canceller and its ACLMS counterpart [20], measured in terms of the digital attenuation ratio, against different transmit powers of FD DCTs.

tions in DC-NCLMS and ANCLMS were both linear in the length of the CIRs to be estimated. The DC-NCLMS required approximately half the computational load of ANCLMS, and this computation efficiency inherent to DC-NCLMS was even more pronounced in the data prewhitening schemes, mainly because the size of the data whitening matrix $\mathbf{\Phi}$ used in the proposed DPA-DC-NCLMS is a quarter of its counterpart for DPA-ANCLMS. The computational complexity of DC-NCAP, on the other hand, was severely influenced by the number of observations, K, mainly because its required multiplications grow cubically with K, as evidenced by Table 1.

In the final set of simulations, we considered digital SI attenuation capabilities of the proposed DC-NCLMS SI canceller, in the steady state stage. Fig. 6 illustrates the digital SI attenuation ratio achieved by DC-NCLMS against different transmit powers. The digital attenuation ratio is a measure of the amount of SI interference before and after applying a canceller, defined as the power ratio between the observed signal $d(n)$ and its output error $e(n)$ [19]. The step-size μ was set to $0.05\mu_{\text{MAX}}$ and $0.2\mu_{\text{MAX}}$, respectively. For comparison, the simulations results for the conventional ACLMS canceller [20] with same step-sizes are also provided. Both the considered cancellers exhibited very similar performance when the transmit power was below 10 dBm. However, as the transmit power became larger, the performance advantages of DC-NCLMS over ACLMS were much more obvious. This is because both the nonlinear SI component, $x_{\text{IMD}}(n)$, and its image became the dominant interference in the high transmit power range, and these were not considered within ACLMS for implementation simplicity. However, due to the inherent consideration for these components within the underlying estimation framework, the proposed DC-NCLMS SI canceller was still able to achieve a sufficient degree of SI attenuation, and its accurate theoretical performance evaluation against different transmit powers can also be observed.

7. Conclusion

A novel dual channel nonlinear complex least-mean-square (DC-NCLMS) based digital self-interference (SI) canceller has been proposed for full-duplex direct-conversion transceivers (FD DCTs) in order to jointly suppress the SI component and its image interference, as well as their nonlinear effects due to major circuitry imperfections, such as frequency-dependent I/Q imbalance and nonlinear power amplifier (PA) distortion. By virtue of the recently introduced complex dual channel (CDC) framework, the proposed DC-NCLMS SI canceller has been established by performing two independent optimisation processes, while still achieving optimal digital SI cancellation performance, but with reduced computational complexities as compared with the augmented nonlinear complex least-mean-square (ANCLMS) digital SI canceller. Comprehensive convergence and steady state performance evaluations of the proposed DC-NCLMS SI canceller have been conducted and have established second order optimality of DC-NCLMS in this context. To further speed up its convergence, both an affine projection based scheme and a data prewhitening one have been introduced. Simulations in practical FD DCT settings, compliant with orthogonal frequency division multiplexing (OFDM)-based IEEE 802.11ac standards, have validated the theoretical findings and have demonstrated the remarkable SI attenuation capabilities of DC-NCLMS.

Acknowledgements

This work was partially supported by the China Scholarship Council (CSC), the National Natural Science Foundation of China under Grant 61771124, and the Zhi Shan Young Scholar Program of Southeast University.

References

[1] J.G. Andrews, S. Buzzi, W. Choi, S.V. Hanly, A. Lozano, A.C.K. Soong, J.C. Zhang, What will 5g be? IEEE J. Sel. Areas Commun. 32 (6) (2014) 1065–1082.
[2] D. Kim, H. Lee, D. Hong, A survey of in-band full-duplex transmission: from the perspective of PHY and MAC layers, IEEE Commun. Surv. Tutor. 17 (4) (2015) 2017–2046.
[3] K.E. Kolodziej, J.G. McMichael, B.T. Perry, Multitap RF canceller for in-band full-duplex wireless communications, IEEE Trans. Wirel. Commun. 15 (6) (2016) 4321–4334.
[4] A. Sabharwal, P. Schniter, D. Guo, D.W. Bliss, S. Rangarajan, R. Wichman, In-band full-duplex wireless: challenges and opportunities, IEEE J. Sel. Areas Commun. 32 (9) (2014) 1637–1652.
[5] J. Choi, M. Jain, K. Srinivasan, Achieving single channel, full duplex wireless communication, in: Proc. ACM MOBICOM, 2010. Pp. 1–12
[6] M. Jain, J.I. Choi, T. Kim, D. Bharadia, S. Seth, K. Srinivasan, P. Levis, S. Katti, P. Sinha, Practical, real-time, full Duplex Wireless, in: Proc. ACM MOBICOM, 2011, pp. 301–312.
[7] M. Duarte, A. Sabharwal, Full-duplex wireless communications Using Off-the-shelf radios: feasibility and first results, in: Proc. 44th Asilomar Conf. Signals, Syst., Comput. (ASILOMAR), 2010. Pp. 1558–1562
[8] T. Riihonen, S. Werner, R. Wichman, Mitigation of loopback self-interference in full-duplex MIMO relays, IEEE Trans. Signal Process 59 (12) (2011) 5983–5993.
[9] E. Antonio-rodríguez, S. Werner, R. López-valcarce, T. Riihonen, Wideband full-duplex MIMO relays with blind adaptive self-interference cancellation, Signal Process 130 (2017) 74–85.
[10] D. Bharadia, E. McMilin, S. Katti, Full duplex radios, ACM SIGCOMM Cmpt. Commun. Rev. 43 (4) (2013) 375–386.
[11] D. Bharadia, S. Katti, I. Nsdi, Full Duplex MIMO Radios, in: Proc. 11th USENIX Symp. NSDI, 2014. Pp. 359–372
[12] E. Everett, A. Sahai, A. Sabharwal, Passive self-interference suppression for full-duplex infrastructure nodes, IEEE Trans. Wirel. Commun. 13 (2) (2014) 680–694.
[13] A. Sahai, S. Diggavi, A. Sabharwal, On Degrees-of-freedom of Full-duplex Uplink/downlink Channel, in: Proc. IEEE ITW, 2013. Pp. 1–5
[14] D. Korpi, J. Tamminen, M. Turunen, T. Huusari, Y.S. Choi, L. Anttila, S. Talwar, M. Valkama, Full-duplex mobile device: pushing the limits, IEEE Commun. Mag. 54 (9) (2016) 80–87.
[15] B. Razavi, Design considerations for direct-conversion receivers, IEEE Trans. Circuits Syst. II 44 (6) (1997) 428–435.
[16] A.A. Abidi, Direct-conversion radio transceivers for digital communications, IEEE J. Solid-State Circuits 30 (12) (1995) 1399–1410.
[17] M. Duarte, C. Dick, A. Sabharwal, Experiment-driven characterization of full-duplex wireless systems, IEEE Trans. Wirel. Commun. 11 (12) (2012) 4296–4307.
[18] Y.S. Choi, H. Shirani-Mehr, Simultaneous transmission and reception: algorithm, design and system level performance, IEEE Trans. Wirel. Commun. 12 (12) (2013) 5992–6010.
[19] D. Korpi, L. Anttila, V. Syrjala, M. Valkama, Widely linear digital self-interference cancellation in direct-conversion full-duplex transceiver, IEEE J. Sel. Areas Commun. 32 (9) (2014) 1674–1687.
[20] M. Sakai, H. Lin, K. Yamashita, Self-interference cancellation in full-duplex wireless with IQ imbalance, Phys. Commun. 18 (2016) 2–14.
[21] S. Li, R.D. Murch, An investigation into baseband techniques for communication systems, IEEE Trans. Wirel. Commun. 13 (9) (2014) 4794–4806.
[22] Z. Li, Y. Xia, W. Pei, K. Wang, Y. Huang, D.P. Mandic, Noncircular measurement and mitigation of i/q imbalance for OFDM-based WLAN transmitters, IEEE Trans. Instrum. Meas. 66 (3) (2017) 383–393.

[23] B. Picinbono, P. Chevalier, Widely linear estimation with complex data, IEEE Trans. Signal Process 43 (8) (1995) 2030–2033.
[24] Y. Xia, D.P. Mandic, Augmented performance bounds on strictly linear and widely linear estimators with complex data, IEEE Trans. Signal Process 66 (2) (2018) 507–514.
[25] Y. Xia, S.C. Douglas, D.P. Mandic, Adaptive frequency estimation in smart grid applications: exploiting noncircularity and widely linear adaptive estimators, IEEE Signal Process. Mag. 29 (5) (2012) 44–54.
[26] Y. Xia, D. Mandic, Complementary mean square analysis of augmented CLMS for second order noncircular gaussian signals, IEEE Signal Process. Lett. 24 (9) (2017) 1413–1417.
[27] Y. Xia, S.C. Douglas, D.P. Mandic, Performance analysis of the deficient length augmented CLMS algorithm for second order noncircular complex signals, Signal Process 144 (2018) 214–225.
[28] Z. Li, Y. Xia, W. Pei, K. Wang, D.P. Mandic, An augmented nonlinear LMS algorithm for digital self-interference cancellation in direct-conversion full-duplex transceivers, IEEE Trans. Signal Process 66 (15) (2018) 4065–4078.
[29] C. Jahanchahi, S. Kanna, D. Mandic, Complex dual channel estimation: cost effective widely linear adaptive filtering, Signal Process 104 (2014) 33–42.
[30] M. Xiang, C.C. Took, D.P. Mandic, Cost-effective quaternion minimum mean square error estimation: from widely linear to four-channel processing, Signal Process 136 (2017) 81–91.
[31] D.P. Mandic, S. Still, S.C. Douglas, Duality between widely linear and dual channel adaptive filtering, in: Proc. IEEE Int. Conf. Acoust., Speech, Signal Process. (ICASSP), 2009. Pp. 1729–1732
[32] L. Anttila, D. Korpi, E. Antonio-Rodríguez, R. Wichman, M. Valkama, Modeling and Efficient Cancellation of Nonlinear Self-interference in MIMO Full-duplex Transceivers, in: Proc. Globecom Workshops, IEEE, 2014. Pp. 777–783
[33] S. Wei, D.L. Goeckel, P.A. Kelly, Convergence of the complex envelope of bandlimited OFDM signals, IEEE Trans. Inf. Theory 56 (10) (2010) 4893–4904.
[34] Pasternack, Datasheet of PE15a1019 amplifier. [Online]. Available: https://www.fairviewmicrowave.com/images/productPDF/SPA-110-30-04-SMA.pdf.
[35] A. devices, Datasheet of HMC619LP5/619LP5e amplifier. [Online]. Available: https://www.analog.com/media/en/technical-documentation/data-sheets/hmc619.pdf.
[36] D. Korpi, T. Riihonen, V. Syrjälä, L. Anttila, M. Valkama, R. Wichman, Full-duplex transceiver system calculations: analysis of ADC and linearity challenges, IEEE Trans. Wirel. Commun. 13 (7) (2014) 3821–3836.
[37] D.P. Mandic, S.L. Goh, Complex valued nonlinear adaptive filters: noncircularity, Widely Linear and Neural Models, John Wiley & Sons, 2009.
[38] S. Javidi, M. Pedzisz, S.L. Goh, D.P. Mandic, The Augmented Complex Least Mean Square Algorithm with Application to Adaptive Prediction Problems, in: Proc. 1st IARP Workshop Cogn. Inform. Process, 2008, pp. 54–57.
[39] K. Kreutz-Delgado, The complex gradient operator and the CR-calculus, ArXiv preprint arXiv: 0906.4835.
[40] S.S. Haykin, Adaptive filter theory, Pearson Education India, 2008.
[41] H. Zhao, Y. Yu, S. Gao, X. Zeng, Z. He, A new normalized LMAT algorithm and its performance analysis, Signal Process 105 (2014) 399–409.
[42] S.C. Douglas, D.P. Mandic, Performance analysis of the conventional complex LMS and augmented complex LMS algorithms, in: Proc. IEEE Int. Conf. Acoust., Speech, Signal Process. (ICASSP), 2010, pp. 3794–3797.
[43] D.P. Mandic, S. Kanna, S.C. Douglas, Mean square analysis of the CLMS and ACLMS for non-circular signals: the approximate uncorrelating transform approach, in: Proc. IEEE Int. Conf. Acoust., Speech, Signal Process. (ICASSP), no. 2, 2015. Pp. pp. 3531–3535
[44] A.H. Sayed, Adaptive filters, 2011. John Wiley & Sons.
[45] J. Ni, X. Chen, Steady-state mean-square error analysis of regularized normalized subband adaptive filters, Signal Process 93 (9) (2013) 2648–2652.
[46] Y. Li, Y. Wang, T. Jiang, Norm-adaption penalized least mean square/fourth algorithm for sparse channel estimation, Signal Process 128 (2016) 243–251.
[47] B. Widrow, S. Stearns, Adaptive Signal Processing, 1985. Prentice Hall, Englewood Cliffs, NJ.
[48] D. Korpi, Y.S. Choi, T. Huusari, L. Anttila, S. Talwar, M. Valkama, Adaptive Nonlinear Digital Self-interference Cancellation for Mobile Inband Full-duplex Radio : Algorithms and RF Measurements, in: Proc. 2015 GLOBECOM, 2015. Pp. pp. 1–7
[49] Y. Xia, C. Took, D. Mandic, An augmented affine projection algorithm for the filtering of noncircular complex signals, Signal Process 90 (6) (2010) 1788–1799.
[50] L. Anttila, M. Valkama, M. Renfors, Circularity-based i/q imbalance compensation in wideband direct-conversion receivers, IEEE Trans. Veh. Technol. 57 (4) (2008) 2099–2113.
[51] Q. Gu, RF System Design of Transceivers for Wireless Communications, Springer-Verlag, New York, NJ, USA, 2006.